ANALYSIS OF HISTORICAL BRIDGES USING THE MIXED DISCRETE ELEMENT METHOD

G. ROUXINOL
Department of Civil Engineering, Polytechnic Institute of Viseu, Portugal
ROUXINOL@DCIVIL.ESTV.IPV.PT
P. PROVIDÊNCIA
Department of Civil Engineering, University of Coimbra, Portugal
provid@dec.uc.pt
V. LEMOS
LNEC – National Laboratory of Civil Engineering, Lisbon, Portugal
vlemos@lnec.pt

ABSTRACT

The discrete element method (DEM) originally applied to the study of jointed rock masses was quickly adapted and generalized to other studies, such as the structural behaviour masonry bridges. This method is well-suited for the representation of predominantly block-discrete structures. The existent formulations consider blocks, rigid or deformable, or by rigid particles. To enlarge its domain of application a rigid mixed plane model of discrete elements was developed, including both blocks and particles. This makes it possible to analyse a masonry arch bridge, modelling the arch and the spandrel walls with blocks and the fill with particles. This model follows the classic specification of the DEM, introducing some new concepts, namely, the definition of a new type of contact and the generation of the mesh of particles. The developed 2D algorithm allows the determination of the eigenvalues and eigenvectors of the structure, which is useful to calibrate the numerical model. The application of the mixed discrete element method to the quasi-static analysis of structures is specially indicated for the calculation of the bearing capacity and respective collapse mode of masonry arches bridges, and an example of this type is presented.

1 INTRODUCTION

This communication presents the numerical mixed discrete elements method (MDEM) for the plane case. This formulation is termed “mixed” because it includes both polygonal discrete elements and circular discrete elements. It was developed in the last three years by the first of the authors while preparing his PhD thesis [1]. The algorithm was translated into a computer program written with Compaq Visual FORTRAN [2], due to the tradition of use of this computer language by the structural engineering research community. The method follows closely the discrete element method (DEM) for blocks [3] and for particles [4] and its main application is the calculation of the load capacity of masonry arch bridges.

The plane model developed includes rigid discrete elements (DE) whose geometry is either polygonal, of three to five vertices, which are referred to in the text by “blocks”, or circular, which are referred by “particles”. Each element may have up to three degrees of freedom, two translational and one rotational components. Each block is geometrically defined by the vertices’ Cartesian coordinates and each particle is defined by its radius and the coordinates of its centre of mass. All the geometric properties are calculated from this data.

The mechanical interaction between the discrete elements is represented by deformable point contacts associated to a constitutive law. Thus, in what can be thought of as part of a

discretization process, the surface of each block is replaced by a finite number of suitably located points, which are the potential contact points. One contact is established whenever one of those potential contact points crosses the external envelope of a nearby discrete element. The interaction forces developed in this contact point are a function of the resulting interpenetration of the two contacting elements. The constitutive model for the contact interface can be formulated in terms of either stresses or resultant forces. The stress formulation is more appropriated when the stress evolution needs to be thoroughly quantified, as is the cases of large discontinuities in massive rocks or when the displacements' history is determining. The formulation by forces is simpler and can be selected for the determination of the collapse load of structures because the local deformability is not critical for the determination of the collapse mechanisms. Note that for the DEM with rigid discrete elements the contacts' deformability embodies the deformability of the whole structural system and thus it should be calibrated through lab tests to guaranty an adequate global behaviour.

In general terms, the DEM consists in the alternate application of the law of motion at the level of the elements and a constitutive law at the level of the contacts. In each iteration the law of motion gives the generalized displacements of the discrete elements and the constitutive law defined by a displacement-force relation gives the contact forces associated to these generalized displacements.

The sections 2 to 6 describe the MDEM, including the motion law, contact's constitutive law, contact definition, detection and updating, critical time step computation and the automatic mesh generation. Section 7 illustrates the application of the method with an example.

2 MOTION OF THE DISCRETE ELEMENTS

In the global coordinates reference system the motion of the mass centre of each discrete element requires the consideration of two translational and one rotational components, (u_1, u_2, θ). The three equations of movement are given by

$$\begin{cases} F_i = m \ddot{u}_i & , \quad i = 1,2 \\ M = I \dot{\omega} \end{cases} \tag{2.1}$$

where u_i and ω are the displacement components and the angular velocity of the centre of mass, m and I are inertial properties of the discrete element and each dot denotes one derivative with respect to time t. The resulting force components, F_i, and moment, M, referred to the centre of mass are given by

$$\begin{aligned} F_i &= F_i^D + F_i^G + F_i^C + F_i^Q = F_i^D + \bar{F}_i \\ M &= M^D + M^C + M^Q = M^D + \bar{M} \end{aligned} \tag{2.2}$$

where F_i^D and M^D are the generalised damping forces, F_i^C and M^C result from the contact forces, F_i^G refers to the mass forces and F_i^Q and M^Q result from other externally applied forces .

For a quasi-static analysis, the DEM requires the inclusion of numerical damping in the equation of motion in order to dissipate the kinetic energy, which allows to consider this as a dynamical relaxation method. Three types of damping where considered: constant global viscous [5], adaptive global viscous [6] and local non-viscous [7]. For the particle mesh definition the inertial properties where also modified in order to optimize the number of iterations the method requires to converge. For this last case, due to the immateriality of

time for a quasi-static analysis, the time step is fixed and the value for the inertial quantities results from the stability condition.

This DEM uses the explicit (finite) central differences method for the time integration of the motion equations (2.1) [8]. Because explicit methods are only conditionally stable, the time step Δt can not exceed a maximum value usually named critical time step which depends of the largest frequency, see section 5.

The central differences scheme gives

$$\ddot{u}_i^t = \frac{1}{\Delta t}\left(\dot{u}_i^{t+\Delta t/2} - \dot{u}_i^{t-\Delta t/2}\right), \quad \dot{\omega}^t = \frac{1}{\Delta t}\left(\omega^{t+\Delta t/2} - \omega^{t-\Delta t/2}\right) \tag{2.3}$$

and

$$\dot{u}_i^{t+\Delta t/2} = \frac{1}{\Delta t}\left(u_i^{t+\Delta t} - u_i^t\right), \quad \omega^{t+\Delta t/2} = \frac{1}{\Delta t}\left(\theta^{t+\Delta t} - \theta^t\right) \tag{2.4}$$

where θ is the rotation of the discrete element (positive in the anti-clockwise direction), and the superscript indicates the time. Using (2.3) the expressions (2.1) are approximated by

$$\dot{u}_i^{t+\Delta t/2} = \dot{u}_i^{t-\Delta t/2} + \frac{F_i^t}{m}\Delta t, \quad \omega^{t+\Delta t/2} = \omega^{t-\Delta t/2} + \frac{M^t}{I}\Delta t \tag{2.5}$$

which give the translational and rotational velocities at the half-step corresponding to time $t + \Delta t/2$. The translational and rotational generalized displacement increments during the time step are given by

$$\Delta u_i^{t+\Delta t} = \dot{u}_i^{t+\Delta t/2}\Delta t, \quad \Delta\theta^{t+\Delta t} = \omega^{t+\Delta t/2}\Delta t \tag{2.6}$$

and, using (2.4), the total generalized displacement are

$$u_i^{t+\Delta t} = u_i^t + \Delta u_i^{t+\Delta t}, \quad \theta^{t+\Delta t} = \theta^t + \Delta\theta^{t+\Delta t} \tag{2.7}$$

Finally, $x_i^{t+\Delta t}$, the new position of the centre of mass of the discrete element is given by

$$x_i^{t+\Delta t} = x_i^t + \Delta u_i^{t+\Delta t} \tag{2.8}$$

The updating of the coordinates, per instance of the vertex A of a block, must include the rotation motion

$$x_i^{\mathrm{A},t+\Delta t} = x_i^{\mathrm{A},t} + \dot{u}_i^{\mathrm{A},t+\Delta t/2}\Delta t\,, \tag{2.9}$$

where $\dot{u}_i^{\mathrm{A},t+\Delta t/2}$ is the velocity of the vertex A which is given by

$$\dot{u}_i^{\mathrm{A},t+\Delta t/2} = \dot{u}_i^{t+\Delta t/2} - e_{ij3}\,\omega^{t+\Delta t/2}\left(x_j^{\mathrm{A},t} - x_j^t\right), \quad i,j = 1,2 \tag{2.10}$$

where e_{ijk} is the permutation symbol.

2.1 Adaptive viscous global damping

Using a damping coefficient proportional to the inertial properties gives the generalized viscous damping forces

$$F_i^{D,t} = -\alpha\, m\, \dot{u}_i^t, \quad M^{D,t} = -\alpha\, I\omega^t \tag{2.11}$$

where α is the viscous damping coefficient. Considering (2.5), (2.2), (2.11) and

$$\dot{u}_i^t \cong \frac{\dot{u}_i^{t-\Delta t/2} + \dot{u}_i^{t+\Delta t/2}}{2}, \quad \omega^t \cong \frac{\omega^{t-\Delta t/2} + \omega^{t+\Delta t/2}}{2}$$

gives

$$\dot{u}_i^{t+\Delta t/2} = \frac{\left(1 - \alpha\,\Delta t/2\right)\dot{u}_i^{t-\Delta t/2} + \dfrac{\bar{F}_i^t}{m}\Delta t}{1 + \alpha\,\Delta t/2}, \quad \omega^{t+\Delta t/2} = \frac{\left(1 - \alpha\,\Delta t/2\right)\omega^{t-\Delta t/2} + \dfrac{\bar{M}^t}{I}\Delta t}{1 + \alpha\,\Delta t/2} \tag{2.12}$$

During the iteration process the initially non-equilibrated generalized forces $\bar{F}_i^t$ and $\bar{M}^t$ will progressively tend to zero with t, in case it converges to a static solution.

In order to reduce the number of iterations required for convergence time the coefficient α should not be kept constant in (2.12). In the adaptive viscous damping formulation [6] this coefficient is varied in such a way that the rate between the damping power and the kinetic energy variation in time $R^t \equiv \sum P^{D,t} \Big/ \left| \sum \dot{E}_k^t \right|$ is kept constant, per instance $R^t = 0.5$, where the sums include all the discrete elements and

$$\begin{aligned} P^{D,t} \big/ \alpha^{\text{avd}} &= I \cdot \left(\omega^t\right)^2 + \sum_{i=1}^{2} m \cdot \left(\dot{x}_i^t\right)^2 \\ 2\Delta t \, \dot{E}_k^t &\cong I \cdot \left(\left(\omega^{t+\Delta t/2}\right)^2 - \left(\omega^{t-\Delta t/2}\right)^2 \right) + \sum_{i=1}^{2} m \cdot \left(\left(\dot{x}_i^{t+\Delta t/2}\right)^2 - \left(\dot{x}_i^{t-\Delta t/2}\right)^2 \right) \end{aligned} \tag{2.13}$$

where α^{avd} is the adaptive viscous damping coefficient. In order to guaranty a gradual variation of α avoid sudden large instead of using the value of α^{avd} resulting from the imposing a constant value to the rate above, the employed value is $\alpha^{t+\Delta t}$ which depends on the difference between the value α^t used in the previous time step and the ideal value α^{avd} by means of

$$\begin{cases} \alpha^{t+\Delta t} = \alpha^t \big/ \delta^i & \text{if} \quad \alpha^{\text{avd}} < \alpha^t \delta^d \\ \alpha^{t+\Delta t} = \alpha^t & \text{if} \quad \alpha^t \delta^d \le \alpha^{\text{avd}} < \alpha^t \big/ \delta^d \\ \alpha^{t+\Delta t} = \min\left(\alpha^t \delta^i, \alpha^0\right) & \text{if} \quad \alpha^{\text{avd}} \ge \alpha^t \big/ \delta^d \end{cases} \tag{2.14}$$

with $\delta^i = 1.05$ e $\delta^d = 0.90$. Because the initial value α^0 is too large the coefficient employed will be progressively reduced. But if an oscillation of the motion suddenly appears it will be gradually incremented. Nevertheless, note that α is not allowed to ever surpass α^0, because that could originate an extremely small time step. As the structural system tends to a steady state (either resting static equilibrium or collapse) the coefficient suffer progressive reduction, reducing the computation time.

2.2 Local non-viscous damping

This formulation uses the following non-viscous damping forces

$$F_i^{D,t} = -\operatorname{sgn}\left(\dot{x}_i^{t-\Delta t/2}\right) \beta \left| F_i^t \right|, \quad M^{D,t} = -\operatorname{sgn}\left(\omega^{t-\Delta t/2}\right) \beta \left| M^t \right| \tag{2.15}$$

where $\operatorname{sgn}\left(f(x)\right) \equiv f(x) \big/ \left| f(x) \right|$ is the sign function and β is a non-viscous damping coefficient. Introducing definitions (2.15) in (2.5) gives

$$\begin{aligned} \dot{x}_i^{t+\Delta t/2} &= \dot{x}_i^{t-\Delta t/2} + \left(1 - \beta \operatorname{sgn}\left(\dot{x}_i^{t-\Delta t/2} \cdot \bar{F}_i^t\right)\right) \frac{\bar{F}_i^t}{m} \Delta t \\ \omega^{t+\Delta t/2} &= \omega^{t-\Delta t/2} + \left(1 - \beta \operatorname{sgn}\left(\omega^{t-\Delta t/2} \cdot \bar{M}^t\right)\right) \frac{\bar{M}^t}{I} \Delta t \end{aligned} \tag{2.16}$$

For the coefficient β [9] and [10] propose the values of 0.8 and 0.7 for systems of, respectively, blocks and particles. For the mixed method treated in this communication the first of those values has been used with success.

2.3 Mass scaling

The mass scaling, in the case of a quasi-static analysis, consists in the use of fictitious values for the inertial quantities [11], reducing the number of iterations required to attain the equilibrium, or collapse, for a pre-defined admissible error. These fictitious values are

obtained multiplying the real ones by a scale factor. As referred above, due to the conditional stability of the integration scheme adopted, the time step to be used must be smaller than a critical value, i.e.

$$\Delta t \le \Delta t_{\text{cr}} = \frac{T_{\min}}{\pi} \cong 2\varphi \cdot \min\left(\sqrt{\frac{m_{\min}}{k_{\max}^{\text{tr}}}}, \sqrt{\frac{I_{\min}}{k_{\max}^{\text{rot}}}} \right) \tag{2.17}$$

with $\varphi \in]0,1]$ and where $T_{\min}$ is the minimum period of the structural system and the point translational and rotational stiffnesses are given by

$$k^{\text{tr}} = 2\sum_{i=1}^{C}\left(k_{s,i} + k_{n,i}\right), \quad k_{\text{block}}^{\text{rot}} = 2r^2\sum_{i=1}^{C}\left(k_{s,i} + k_{n,i}\right), \quad k_{\text{particle}}^{\text{rot}} = 2r^2\sum_{i=1}^{C}k_{s,i}$$

where C is the total number of contacts of each discrete element and the subscripts s and n denote the contact shear and normal directions, k_s, k_n being thus the corresponding initial elastic stiffnesses, see [11]. Expression (2.17) shows that if the inertial properties m and I are increased the time step is also increased. Per instance, the critical time step can be increment up to $\Delta t_{\text{cr}}^{\text{ms}}$ if the real inertial properties are multiplied by,

$$\frac{m_{\min}^{\text{ms}}}{m_{\min}}, \frac{I_{\min}^{\text{ms}}}{I_{\min}} = \left(\frac{\Delta t_{\text{cr}}^{\text{ms}}}{\Delta t_{\text{cr}}}\right)^2 \tag{2.18}$$

When, during the iterative process, the contacts are updated C can be modified which implies updating also $\Delta t_{\text{cr}}^{\text{ms}}$.

3 CONSTITUTIVE FORCE-DISPLACEMENT LAW

Each contact has a pair of opposite normal (compression) forces and a pair of opposite shear (or tangential) forces acting on the two contacting elements. The magnitudes of these forces depend upon the constitutive law and the magnitudes of the normal and tangential relative displacements. If, at time t, the coordinates of the contact point C are $x_j^{C,t}$ the velocity at time $t+\Delta t/2$ of this contact point C for the discrete element $\mathbf{X}$ (which denotes one of the two contacting elements $\mathbf{A}$ and $\mathbf{B}$), is given by,

$$v_i^{C,\mathbf{X},t+\Delta t/2} = v_i^{\mathbf{X},t+\Delta t/2} - e_{ij3}\,\omega^{\mathbf{X},t+\Delta t/2}(x_j^{C,t} - x_j^{\mathbf{X},t}), \quad i,j = 1,2 \tag{3.1}$$

where, when standing alone, the superscript $\mathbf{X}$ refers to the centre of mass of the element. In the case of a contact involving one vertex of a block (or two) the velocity of the contact point, which does not coincide with the vertex, see [12], can be approximated by (2.10). At the contact point C the relative velocity between the two discrete elements as components $v_i^C = v_i^{\mathbf{B},C} - v_i^{\mathbf{A},C}$, where, for simplification, the reference to time will be omitted in the following. For a local system of coordinates associated to the contact's principal directions, the tangential (shear) and normal components of the relative velocity is

$$\begin{Bmatrix} v_s^C \\ v_n^C \end{Bmatrix} = \left(\overline{\mathbf{n}}^C\right)^{\text{T}} \begin{Bmatrix} v_1^C \\ v_2^C \end{Bmatrix}, \quad \overline{\mathbf{n}}^C = \begin{bmatrix} n_2 & n_1 \\ -n_1 & n_2 \end{bmatrix} \tag{3.2}$$

where n_i are the components of the contact's normal in the global system of coordinates, which is an unitary vector pointing from the DE with the smaller reference label to the DE with the larger reference label, see [1]. The contact's relative displacement increment during a time step, which is given by the difference between the displacements of the contacting elements on the contact point, is approximated by

$$\begin{Bmatrix} \Delta u_s^C \\ \Delta u_n^C \end{Bmatrix} = \Delta t \begin{Bmatrix} \Delta v_s^C \\ \Delta v_n^C \end{Bmatrix} \tag{3.3}$$

and the corresponding tangential and normal (compression positive) force increments are

$$\begin{Bmatrix} \Delta F_s^C \\ \Delta F_n^C \end{Bmatrix} = -\begin{bmatrix} k_s & 0 \\ 0 & k_n \end{bmatrix} \begin{Bmatrix} \Delta u_s^C \\ \Delta u_n^C \end{Bmatrix} \tag{3.4}$$

If the time step is small enough for ignoring the effect of the rotation of the local system of coordinates in the following sum, the total tangential and normal contact forces would be

$$\begin{Bmatrix} F_s^C \\ F_n^C \end{Bmatrix}^* = \begin{Bmatrix} F_s^C \\ F_n^C \end{Bmatrix} + \begin{Bmatrix} \Delta F_s^C \\ \Delta F_n^C \end{Bmatrix} \tag{3.5}$$

where the superscript * denotes that these are not definitive values because the strength criteria must still be considered: (1) if $F_n^{C*} < 0$ the contact becomes virtual and $F_s^C = F_n^C = 0$; (2) if the value of the compression surpasses the maximum allowable stress of any of the two contacting elements this maximum value is imposed; (3) if $\left|F_s^{C*}\right| > F_{s,\max}$, $F_s^C = \operatorname{sgn}\left(F_s^{C*}\right) \cdot F_{s,\max}$, where, if $F_n^C > 0$, the maximum shear force is defined by the Mohr-Coulomb's criterion $F_{s,\max} = c + F_n^C \tan\phi$, c, ϕ being the cohesion and angle of friction. The generalized forces, associated to the centre of mass of the discrete elements, due to the contact phenomena are defined by

$$\begin{cases} F_i^{\mathbf{A}} = -F_i^C \\ M^{\mathbf{A}} = e_{ij3} F_i^C \left(x_j^C - x_j^{\mathbf{A}}\right) \end{cases}, \quad \begin{cases} F_i^{\mathbf{B}} = F_i^C \\ M^{\mathbf{B}} = -e_{ij3} F_i^C \left(x_j^C - x_j^{\mathbf{B}}\right) \end{cases}, \quad i, j = 1, 2, \quad \begin{Bmatrix} F_1^C \\ F_2^C \end{Bmatrix} = \overline{\mathbf{n}}^C \begin{Bmatrix} F_s^C \\ F_n^C \end{Bmatrix} \tag{3.6}$$

4 MECHANICAL INTERACTION BETWEEN THE DISCRETE ELEMENTS

The model of the mechanical interaction between two discrete elements at a contact point is described in the previous section. A simple and systematic definition of the contacts is required in order to guaranty the consistence of the geometric relations and the efficiency of the contact detection method. As an example of the consequences of this requirement, in order to allow for an unambiguous definition of the contacts, the vertices of the blocks are regularized using circular arches which are tangent to the adjacent sides [13] and whose centre are named *theoretical vertices*, see Figure 1.

4.1 Contacts' geometry

There are eight different types of contacts: (1) corner-corner; (2) corner-edge; (3) edge-corner; (4) circle-circle; (5) corner-circle; (6) edge-circle; (7) circle-corner; (8) circle-edge, where the terms corner and edge are used for blocks and the term circle for particles. Each contact is characterised by eight data items: (1) the numbered contact reference label C_i (i = 1, …, number of contacts); (2) the contact type Γ_i^C; (3) the contact point coordinates $\mathbf{x}_i^C \equiv x_{i,j}^C, \left(j = 1, 2\right)$; (4) the components of the contact surface's normal $\mathbf{n}_i \equiv n_{i,j}^C$; (5) the numbered reference labels of the two interacting discrete elements, $\left\{\mathbf{A}_i, \mathbf{B}_i\right\}$ with $\mathbf{A}_i < \mathbf{B}_i$ (the subscript i will be normally omitted); (6) the coordinates of the centres of mass of the interacting discrete elements, $\mathbf{x}_i^{\mathbf{A}}, \mathbf{x}_i^{\mathbf{B}} \equiv x_{i,j}^{\mathbf{A}}, x_{i,j}^{\mathbf{B}}$; (7) and (8) the coordinates of each vertex $\mathbf{x}_i^{\mathrm{A}}, \mathbf{x}_i^{\mathrm{B}} \equiv x_{i,j}^{\mathrm{A}}, x_{i,j}^{\mathrm{B}}$ and of each theoretical vertices $\mathbf{x}_i^A, \mathbf{x}_i^B \equiv x_{i,j}^A, x_{i,j}^B$ of the contacting elements. A *virtual* contact is established, before real contact occurs, whenever the distance between two elements becomes smaller than a predefined tolerance distance, in order to reduce the number of times the contact detection subroutines are accessed, because these are quite greedy in terms of computing time. The contact forces exist only for *real* contacts, which correspond to effective (numerical) overlapping and null (physical) gap or separation. A local rectangular system of coordinates $(t, n)^C$ is defined for contact

C, whose origin is located on the contact point and whose normal axis is perpendicular to the surface of contact, see Figure 1. The type classification of the contact results is defined by two geometrical conditions. For a type 1 contact there are two vertices potentially in contact, A and B, and the geometrical conditions are (a) the projection of the theoretical vertex B on the edges adjacent to A must fall inside the circular region and vice versa; (b) the discrete elements superposition d^C (negative when effective overlapping or superposition occurs) must satisfy two admissible tolerances $d_O > 0$ and $d_G < 0$, the first one controlling effective contact and the second effective separation,

$$-d_O < d^C < d_G \ , \ d^C = \overline{AB} - R_A - R_B \tag{4.1}$$

For contacts of types 4, 5 and 7 the criteria are similar to those above, but simpler as it may be unnecessary to verify if the contact occurs in a circular region. For contacts of types 2, 3, 6 and 8 similar geometric conditions apply. For instance, for a type 2 contact the projection of the theoretical vertex A over the edge adjacent to vertex B must fall outside the corresponding circular arch and the conditions (4.1) are satisfied for the redefined superposition $d^C = D - R_A$, where D is the distance between the theoretical vertex A and the edge adjacent to vertex B. The contacts of the types 1, 4, 5 and 7 and of the types 2, 3, 6 and 8 have coordinates given by, respectively,

$$\begin{Bmatrix} x_1^C \\ x_2^C \end{Bmatrix} = \begin{Bmatrix} x_1^A \\ x_2^A \end{Bmatrix} + \left(R_A + \frac{d^C}{2} \right) \begin{Bmatrix} n_1^C \\ n_2^C \end{Bmatrix}, \quad \begin{Bmatrix} x_1^C \\ x_2^C \end{Bmatrix} = \begin{Bmatrix} x_1^X \\ x_2^X \end{Bmatrix} - \left(\overline{\mathbf{n}}^e \right)^T \begin{Bmatrix} d_{t1} \\ \dfrac{d^C}{2} \end{Bmatrix}, \quad \overline{\mathbf{n}}^e = \begin{bmatrix} n_2^e & n_1^e \\ -n_1^e & n_2^e \end{bmatrix} \tag{4.2}$$

where $X \equiv A$ for 3 and 6 type contact and $X \equiv B$ for 2 and 8 type contact and $(t,n)^e$ is the local referential whose origin is located on the vertex adjacent to the contacting edge first encountered when rotating in the anti-clockwise direction from the contact point, with n^e perpendicular to this edge. dt_1 is the distance between the vertex adjacent to the contacting edge and the projection of the theoretical vertex on the edge.

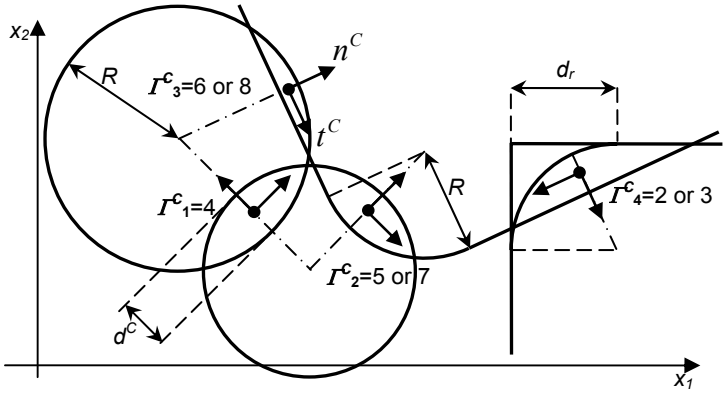

Figure 1 – Types of contact between discrete elements.

4.2 Contacts' detection and updating

During the iterative process the DEM detects automatically when a new contact is created or when a previous contact vanishes. This requires a simple representation of the potentially contacting zones and a robust and efficient numerical algorithm which detects and updates the contacts [11], [14], [15]. The developed detection algorithm is based on Cundall's method [14] and the enveloping volumes method [16]. A rectangular mesh is first represented over the structural domain, see Figure 2, which allows that an incidence matrix with a column for each of the cells formed by the rectangular mesh and a line for each discrete element. Thus all the elements totally or partially contained in a given cell appear in the same column of the incidence matrix. Next each discrete element is circumscribed with a circular envelope, see Figure 2. Then, a cell by cell search of

potential contacts is carried out. In each cell, a envelope by envelope search is made and if two envelopes overlap then a more geometrically accurate local search based on the conditions established in the previous section is performed, which identifies effective contacts.

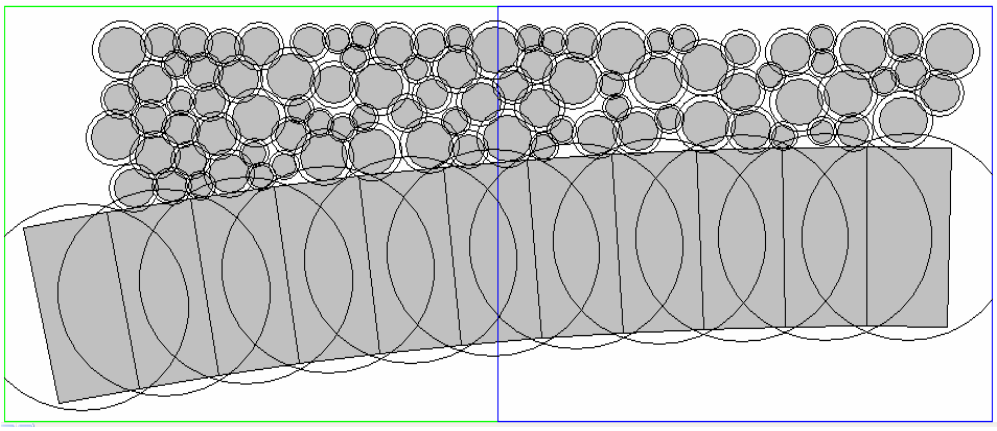

Figure 2 – Rectangular mesh and enveloping volumes.

In order to avoid performing the contact detection in all the iterations the program establishes and keeps track of an approximated value for the maximum accumulated displacement since the last contact detection executed. Whenever this displacement exceeds $\eta\, d_r$ (where d_r is the rounding parameter of the blocks' vertices, see Figure 1), with the coefficient $\eta = 1.1$ by default, a new contact detection is performed and the incidence matrix updated. For systems with many discrete elements, per instance 3D systems or simulation of flows with particles, more advanced methods, per instance using binary trees, should be used.

5 TIME STEP DEFINITION

The selection of the time step Δt is relevant because the overall computational cost is proportional to the total number of iterations required for the process to converge. The stability of the recursive numerical operator an the integration accuracy are the two most important factors to consider when seeking for the maximum allowed value for Δt.

For stability the spectral radius of the recurrent operator must be smaller than the unity. For the direct integration of (2.1) and in order to satisfy the last condition, the conditionally stable central difference scheme requires a time step which satisfies [17], $\Delta t \le \Delta t_{\text{cr}} = T_{\min}/\pi$, where $T_{\min}$ is the minimum non damped period of the DE system. The code developed includes also the capability to perform an eigenvalue analysis, under the assumption of elastic joints, which allows the validation of the simplified formulas adopted in practice. In general the integration accuracy will also be verified if Δt satisfies the previous relation. By considering a regular mesh and a unique DOF global mode with maximum relative displacement at the contacts [18] establishes a simplified expression for $T_{\min}$ which gives

$$\Delta t_{\text{cr}} = 2\lambda\sqrt{m_{\min}/k_{\max}} \qquad (5.1)$$

where the parameter $\lambda \in]0,1[$ accounts for a number of contacts larger than one (in general, use $\lambda \in]0.1,0.5[$), $m_{\min}$ is the minimum DE mass and $k_{\max}$ is the maximum contact stiffness. It is also possible to calculate Δt_{cr} using Gerschgorin theorem [19] to define a maximum value to the frequency as the maximum rate between stiffness and

corresponding inertial property for all the degrees of freedom of the system considered isolated, $\Delta t_{\mathrm{cr}} = \min\left(m/k^{\mathrm{tr}}, I/k^{\mathrm{rot}}\right)$ with $k^{\mathrm{tr}}, k^{\mathrm{rot}}$ as defined in section 2.

To compute Δt_{cr} from the eigenvalue problem it is necessary to calculate the stiffness matrix of the structural system [1]. Because the stiffness of the present model results from the effective point contacts in operating in the elastic range the global stiffness matrix is obtained adding up the contribution of all the eligible contacts, whose elementary stiffness matrix in local coordinates is given by

$$\mathbf{k}^{C} = \begin{bmatrix} k_s & 0 & -d_n^{\mathbf{A}}k_s & -k_s & 0 & d_n^{\mathbf{B}}k_s \\ 0 & k_n & d_s^{\mathbf{A}}k_n & 0 & -k_n & -d_s^{\mathbf{B}}k_n \\ -d_n^{\mathbf{A}}k_s & d_s^{\mathbf{A}}k_n & (d_s^{\mathbf{A}})^2k_n + (d_n^{\mathbf{A}})^2k_s & d_n^{\mathbf{A}}k_s & -d_s^{\mathbf{A}}k_n & -d_s^{\mathbf{A}}d_s^{\mathbf{B}}k_n - d_n^{\mathbf{A}}d_n^{\mathbf{B}}k_s \\ -k_s & 0 & d_n^{\mathbf{A}}k_s & k_s & 0 & -d_n^{\mathbf{B}}k_s \\ 0 & -k_n & -d_s^{\mathbf{A}}k_n & 0 & k_n & d_s^{\mathbf{B}}k_n \\ d_n^{\mathbf{B}}k_s & -d_s^{\mathbf{B}}k_n & -d_s^{\mathbf{A}}d_s^{\mathbf{B}}k_n - d_n^{\mathbf{A}}d_n^{\mathbf{B}}k_s & -d_n^{\mathbf{B}}k_s & d_s^{\mathbf{B}}k_n & (d_s^{\mathbf{B}})^2k_n + (d_n^{\mathbf{B}})^2k_s \end{bmatrix} \tag{5.2}$$

where $d_{n,s}^{\mathrm{X}}$ is the distance from the centre of mass of the discrete element X to the contact point, measured along the local reference system directions.

6 GENERATION OF THE DISCRETE ELEMENTS MESHES

The characterization of the geometry of existing masonry structures can be performed by different methods, either classical, based on reading drawings and/or on measuring through tape, tachometer and laser distance meter; either more recent ones, based on photographic techniques, usually designated by remote sensing (photogrammetry) [20] [21], and in situ tests including ultrasounds [22].

In accordance to these different methods, the geometry of the spatial mesh of discrete elements is obtained either by automatic generation of several types of structural elements based on a few main geometric parameters or by reading ASCII files, like DXF™ (which basically is a tagged graphic data representation format). The standard structural elements include semi-circular arches, segmental (shallow/deep) arches, buttresses, columns, walls, spandrel walls and the fill material.

The mesh of particles, according to the type of fill, allows for regular distributions, either rectangular or hexagonal, and for random distributions, with a constant or variable radius. According to the method of expansion of the radius [23] the generation of the particles' random mesh requires the definition of (1) a rectangular area which defines the main domain as there are no particles in its exterior; (2) a set of withdrawn convex and closed sub domains (circular, rectangular, triangular, circle segment, etc.) which define zones inside the main domain where no particle is accepted. The admissible domain is given by the main domain without the withdrawn sub domains. In order to guaranty a predefined porosity, when they are first randomly distributed all over the admissible domain, the particles possess a reduced radius, Figure 3(a), and only afterwards is the radius expanded. Then, by means of the application of the MDEM the system is allowed to converge to a configuration which corresponds to the predefined porosity (or stress field), Figure 3(b). Before the distribution of the particles a layer of blocks is placed above the pavement level (which corresponds to upper facet of the allowable domain), Figure 3(a). These blocks are removed after the expansion stage. After the conclusion of the definition of the mesh of the discrete elements, it can be visualised either still inside the Compaq

Visual FORTRAN environment or with AutoCAD® [24] through the help of a built-in VBA (Microsoft Visual Basic for Applications) macro.

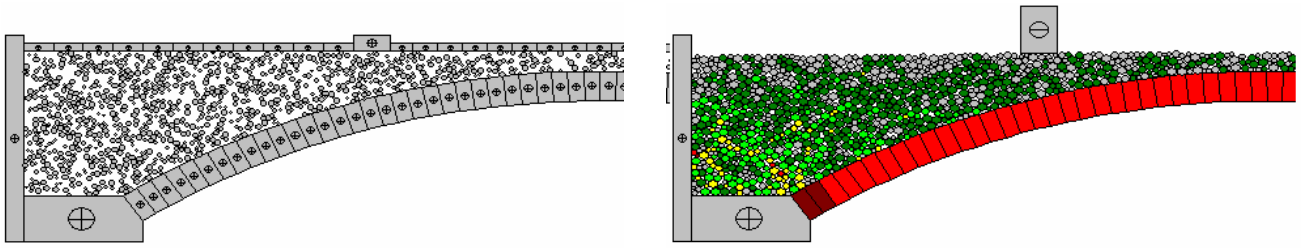

(a) (b)

Figure 3 – Discrete elements mesh (a) before and (b) after the expansion stage.

7 APPLICATION EXAMPLE

This section follows very closely [25] which contains some additional details. The collapse of the Bridgemill masonry arch bridge, built in 1869 at Girvan, Scotland, is studied for the illustration of the presented algorithm. Hendry, Davies et Royles measured its geometry, determined its mechanical properties, performed a load test and registered the value of the load previous to its collapse [26]. Due to the shortage of records of this nature, this example has been used by several researchers in order to validate their numerical models [27]. In the following some considerations about the values selected to the parameters required to define the properties of the structural materials used in the bridge. The discrete element mesh employed models the arch and (the fixed) abutments with blocks and the fill with particles. The numerical collapse load is compared with the in situ value obtained by Hendry. et al [26]. However [26] lacks some decisive parameters. This entailed (1) the selection of some values referred to in the specialized literature for similar structures (2) as well as a controlled estimation of other values in order to improve the numerical results when these are compared with those obtained in situ.

The bridge arch is parabolic with a free span of 18.3 m, 8.3 m width, 2.85 m rise at midspan and it is made of 62 sandstone voussoirs, with a depth h = 0.711 m. For this span/rise ratio the parabola is quite flat, almost coincident with a circular arc, so that it is admitted as a segmental arch [26] [28]. The distance from the keystone extrados to the pavement surface is 0.478 m, including the depth of fill at crown (0.203 m), the sub-base thickness (0.125 m) and the bituminous surfacing (0.150 m).

The voussoirs and the spandrel walls have a density γ_b = 2100 kg / m^3, a deformation modulus E_b = 15 000 MPa and a compressive strength f_b = 43,8 MPa. The fill material, composed from a mixture of gravel, sand and clay, has a density γ_f = 1890 kg / m^3 and a deformation modulus E_f = 40 MPa, [27].

As a first estimate, the normal k_n and the shear k_s contact elastic stiffnesses per unit area, which are equivalent stiffnesses resulting from the combined effect of the blocks and the joint, satisfy,

$$\frac{1}{k_n} = \frac{1}{k'_n} + \frac{l_{cm}}{E_b}; \quad \frac{1}{k_s} = \frac{1}{k'_s} + \frac{l_{cm}}{G_b} \tag{5.1}$$

where l_{cm} is the length defined by the centres of mass of the two contacting blocks (measured along the contact's normal), k'_n and k'_s are the effective joint normal and shear

stiffnesses per unit area and G_b is the blocks' elastic shear modulus [29]. Table 1 gives the values considered for the parameters for the three types of contact, i.e. between blocks b-b, between particles p-p and mixed b-p. The values adopted for $k'_{\_,\text{b-b}}$, $k'_{\_,\text{b-p}}$ and the Poisson's ratio ν refer to Lagoncinha's Bridge, Portugal, and were experimentally determined by Costa [20].

Table 1 – Stiffness of the contacts.

	$l_{\text{c.m.}}$	ν	E	G	k'_n	k'_s	k_n	k_s
	m	—	GPa	GPa	GPa / m	GPa / m	GPa / m	GPa / m
b-b	0.3208	0.2	15.000	6.250	5.400	0.590	4.840	0.573
b-p	0.1500	0.2	15.000	6.250	65.000	27.000	4.840	0.573
p-p	0.1500	0.2	0.040	0.017	65.000	27.000	1.596	0.666

For the b-p contacts formulae (5.1) gave $k_n = 0.079\,\text{GPa/m}$ and $k_s = 0.033\,\text{GPa/m}$, but these values had to be increased ($k_{\_,\text{b-p}} \equiv k_{\_,\text{b-b}}$) in order to avoid excessive superposition. For the p-p contacts the values considered for k'_n and k'_s to those corresponding to the b-p contacts.

The values used for the p-p contact stiffnesses k_n and k_s should be such that the fill's overall rigidity is similar to E_f. In order to calculate them the arbitrary values $k'_{\_,\text{p-p}} \equiv k'_{\_,\text{b-p}}$ were assumed, the values of k_n and k_s specified by (5.1) calculated and referred to as $k_{n,(1)} = 0.266\,\text{GPa/m}$ and $k_{s,(1)} = 0.111\,\text{GPa/m}$. Then a $1\,\text{m}$ side square's sample was isolated from the fill's mesh, Figure 4, replacing, when possible, partially truncated particles by smaller ones. Subsequently this sample was confined with three fixed blocks, placed below and on its sides, Figure 5. A fourth block weighing 2.6 kN and free to move vertically was then subjected to load increments of 25 kN, Figure 5, and its vertical displacement measured, Figure 6. This procedure was performed for values of k_n and k_s given by one, two, four, six and eight times $k_{n,(1)}$ and $k_{s,(1)}$, all the other parameters being kept fixed. The average tangent deformation modulus is respectively 22, 28, 34, 42 and 48 MPa and the secant deformation modulus (difference between first and last results) 16, 26, 12, 14 and 18 MPa. The three last values are significantly higher if the first four load steps are ignored, 28, 43 and 54 MPa, see Figure 6. In order to satisfy the value specified for E_f the stiffnesses adopted for the p-p contacts should be about $k_n = 6\,k_{n,(1)} = 1.596\,\text{GPa/m}$ and $k_s = 6\,k_{s,(1)} = 0.666\,\text{GPa/m}$, see Table 1.

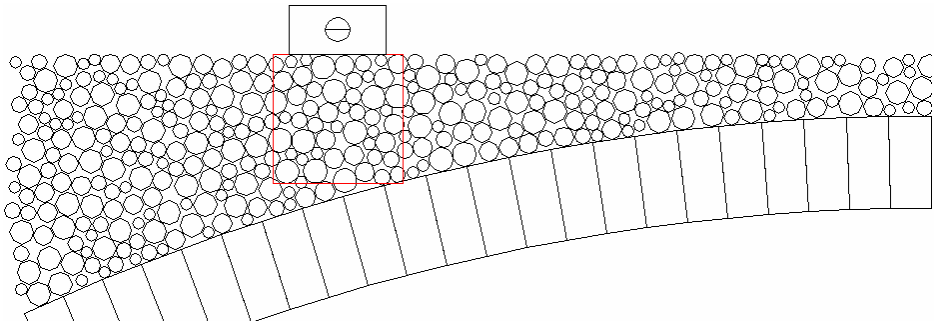

Figure 4 – Definition of the sample of particles.

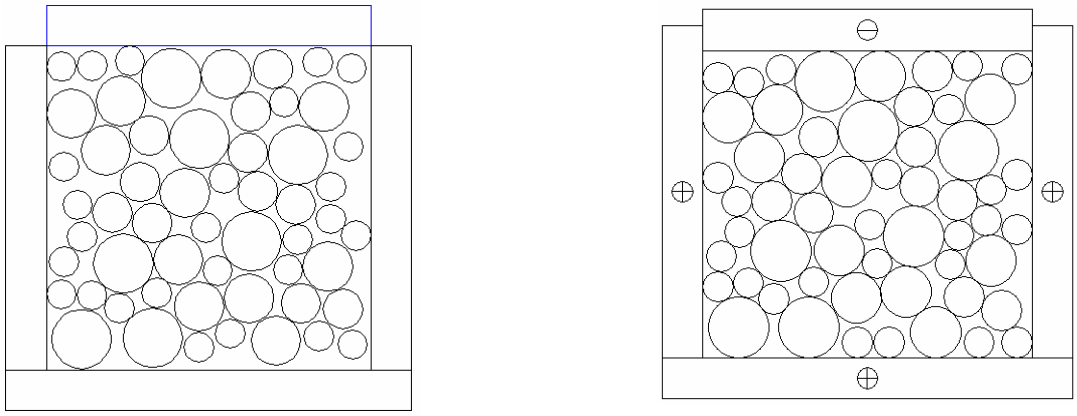

(a) (b)

Figure 5 – (a) Confinement of the sample and (b) loading of the confined sample.

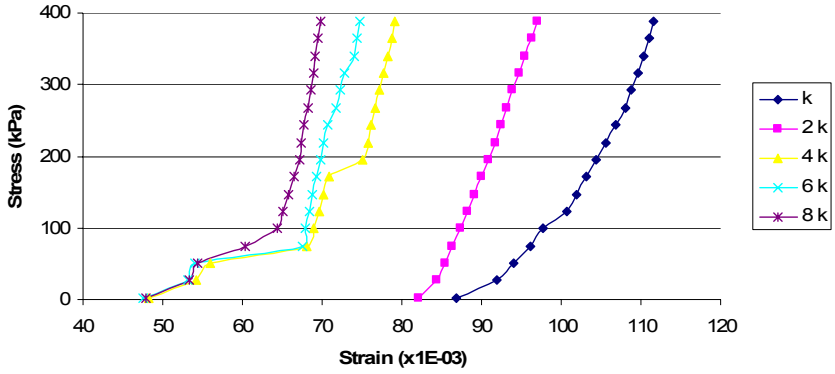

Figure 6 – Stress-strain relation for the confined particles.

Table 2 gives the remaining parameters required. Following [30] and [31] the sandstone tensile strength $f_{b,t}$ is ignored. The fill material's tensile strength $f_{f,t}$ is also ignored. As there is no record of the internal friction angle ϕ, the value used for all types of contact was the one obtained from lab tests for the Serra do Pilar Monastery, Portugal, [32]. For the p-p and b-p contacts a cohesion $c_f = 10\,\text{kPa}$ was adopted, as justified by the values in the range $[1.0, 20.0]\text{kPa}$ specified by [33] e [34], and for the b-b contacts $c_b = 0$. For an analysis per unit width, the contact's influence area is given by $a_c = l_c \times 1 = l_c$, where l_c is the contact's influence length. If l_c is allowed to vary for the b-b contacts, a minimum must be defined and, following Coulomb [35], the value $l_{c,\min} = h_b / 10$ was selected. If l_c is fixed then it is given by (1) for the b-b contacts, half the distance between the contact points along the height of the blocks, $l_{c,\text{fixed}} = (h_b - d_r)/2 = 0.3455\,\text{m}$, (2) for the b-p and p-p contacts, the average of the diameters of the particles.

Table 2: Further properties for the discrete elements and joints.

	c kPa	ϕ °	$f_{b,t}, f_{f,t}$ MPa	$f_{b,1}$ MPa	$l_{c,fixed}$ m	$l_{c,\min}$ m
b-b	0	35.6	0	43.8	0.3455	0.0711
b-p	10	35.6	0	—	0.1500	—
p-p	10	35.6	0	—	0.1500	—

In the following analyses the dead weight of the structure is "applied" first, then the corresponding stable configuration is computed, and only after this are the other loads

applied. The arch's abutments are fixed, and their upper face length is 2.0 m. The arch model contains one block for each voussoir and the fill mesh contains 1984 particles. The point (knife) load is applied at quarter span, by means of an additional block weighing 17.72 kN / m (147 kN) prevented from either rotate or move horizontally, in increments of 200 kN.

For this example the non-viscous local type of numerical damping was used and the contact influence length was kept fixed. The collapse load is 3147 kN, and the maximum compression value was below f_b (2.90 MPa for 2947 kN). Figure 7 compares the load-displacement curve for the quarter span voussoir with the one obtained by Hendry [27]. The qualitative difference between the two curves can be summarized in the difficulty that the MDEM reveals in accommodating the arch's progressive stiffness reduction. This might be a consequence of the adoption of rigid discrete elements or of the purely linear elastic range used in the constitutive law. The subject is still under investigation.

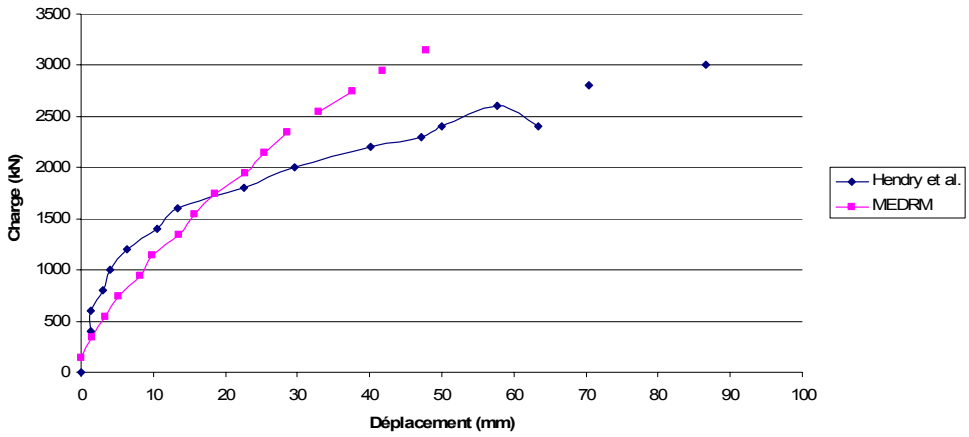

Figure 7 – Load-displacement relations.

Figure 8 to Figure 11 illustrate the collapse mechanism, revealing the prior rupture of the fill material due to the effect of the block that stands the point load and the collapse of the arch for what appears to be an almost direct application of this block on the arch extrados.

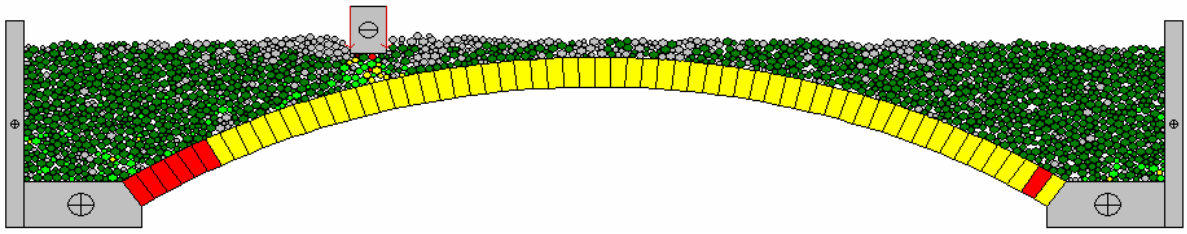

Figure 8 – Mixed discrete element model configuration for $F = 800\ \mathrm{kN}$.

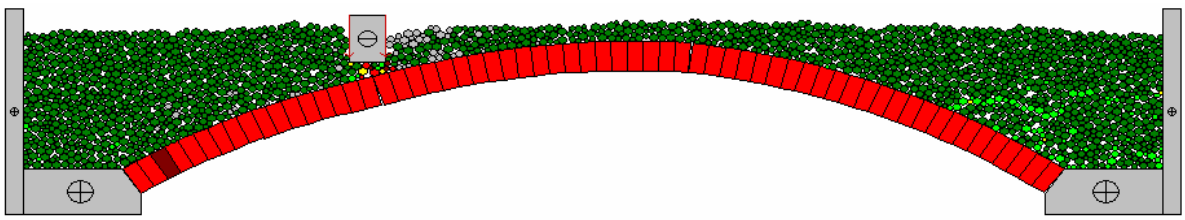

Figure 9 – Configuration for impending collapse.

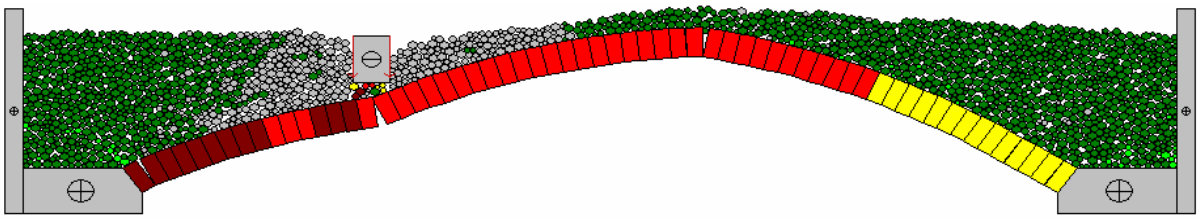

Figure 10 – Configuration for incipient effective collapse.

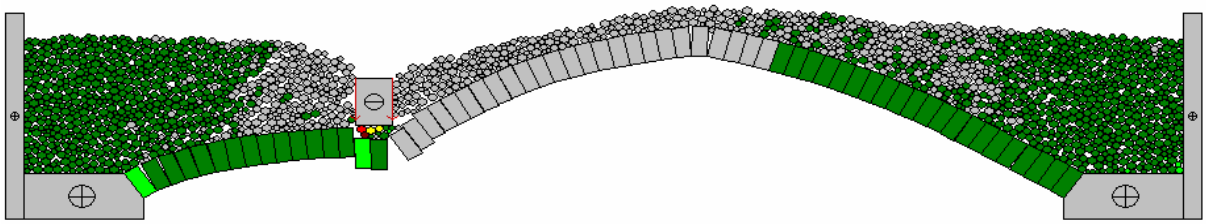

Figure 11 – Configuration for effective collapse.

8 CONCLUSIONS

This communication presents the mixed discrete element method and its application for the numerical computation of the collapse load of masonry arch bridges. The interaction between rigid discrete elements considered includes the new block-particle type of contact. The semi-automatic mesh generation routines are specialized to the major types of discrete elements. The example which concludes the communication illustrates the good performance of this method, which is still under development.

REFERENCES

1. Rouxinol, G. A. F. Structural modelling and evaluation of masonry arch bridges. PhD Thesis in preparation. University of Coimbra, Portugal
2. Compaq Visual Fortran® 6.6 (2002). Program developing software. Compaq Information Technologies Group, L.P
3. Cundall, P. A. (1971). A Computer model for simulating progressive large scale movements in blocky rock systems. Proc. of the Symposium of the Society of Rock Mechanics. Vol 1, paper No II-8, Nancy, France
4. Cundall, P. A. et Strack, O. D. L. (1979). A discrete numerical model for granular assemblies. Géotechnique. Vol 29, No 1, pp 47-65
5. Cundall, P. A. (1971). The Measurement and analysis of accelerations in rock slopes. PhD Thesis, Imperial College, University of London
6. Cundall, P. A. (1982). Adaptive Density-Scaling for Time-Explicit Calculations. Proc. 4th Int. Conf. Numerical Methods in Geomechanics. Edmonton, Canada, pp. 23-26.
7. Cundall, P. A. (1987). Distinct Element Models of Rock and Soil Structure. Analytical and Computational Methods in Engineering Rock Mechanics, ed. Brown, E. T. George Allen & Unwin, pp. 129-163.
8. Hughes, T. J. R. (1987). The finite element method. Prentice-Hall.
9. ITASCA Consulting Group (1999). UDEC – Universal Distinct Element Code, User's Manual. Version 3.1. Minneapolis USA.
10. ITASCA Consulting Group (2002). PFC2D – Particle Flow Code in 2 Dimensions. User's Guide. Version 3.0. Minneapolis, USA.
11. Lemos, J. V. (1999). Modelling and failure analysis in rock engineering. LNEC, Lisbon.
12. Rouxinol, G. A. F., Providência, P. et Lemos, J. V. (2006). The discrete element method with 2D rigid polygonal and circular elements. 5th Conf. on Structural Analysis of Historical Constructions. Eds. Lourenço, P. B. et al. Vol 2, pp 1023-1031, New Delhi, India
13. Sîncraian, G. (1998). A discrete element program based on a rigid block formulation. LNEC, Lisbon.

14. Cundall, P. A. (1988). Formulation of three-dimensional distinct element model – Part I: A scheme to detect and represent contacts in a system composed of many polyhedral blocks. Int. J. Rock Mech. Min. Sci. & Geomech. Abstr 25(3), pp 107-116
15. Munjiza, A (2004), The combined finite-discrete element method. John Wiley & Sons.
16. Williams, J. R. (1988). Contact analysis of large numbers of interacting bodies using discrete modal methods for simulating material failure on the microscopic scale. Eng. Computations 5, pp 198-209
17. Bathe, K.J. (1982). Finite element procedures in engineering analysis, Prentice-Hall.
18. Morikawa, H., Sawamoto, Y. and Kobayashi, N. (1993). Local Fracture Analysis of a Reinforced Concrete Slab by the Discrete Element Method. Proc. 2nd Int. Conf. Discrete Element Methods, pp. 275-286. USAIESL Publications, Cambridge
19. Underwood, P. (1983). Dynamic relaxation. Computational Methods for Transient Analysis. In Computational Methods for Transient Analysis, eds. Belytschko, T. and Hughes, J. R. North-Holland, pp.1-65.
20. Costa, C. (2002). Analysis of the behaviour of bridge of Lagoncinha under automobile traffic. M.Sc. Thesis, University of Porto, Portugal (in Portuguese)
21. Valença, J. (2006). Photogrammetric techniques in structural engineering. M.Sc. Thesis, University of Coimbra, Portugal (in Portuguese)
22. Komeyli-Birjandi, F. (1986). Sonic investigation of masonry structures, PhD Thesis, University of Edinburgh
23. Potyondy, D. O. and Cundall, P. A. (2004). A bonded-particle model for rock. Rock Mech. Min. Sci., n 41, pp. 1329-1364
24. AutoCAD® 2007 3D (2006). Computer Aided Design. Autodesk, USA.
25. Rouxinol, G. A. F., Providência, P. et Lemos, J. V. (2007). Bridgemill bridge bearing capacity assessment by a discrete element method. Submitted to the 5th Int. Conf. Arch Bridges, Madeira, Portugal
26. Page, J. (1993). Masonry arch bridges. State-of-the-Art Review. Transport Research Laboratory, Department of Transport, London
27. Molins, C. (1998). Numerical simulation of the response of arch Bridgs. In Proc. 2nd Int. Seminar Structural Analysis of Historical Constructions, Eds. P. Roca et al. CIMNE, Barcelona pp. 93-123
28. Vermeltfoort, A.T. (2001). Analysis and experiments of masonry arches. In Historical Construction, Eds. Lourenço, P. B. and Roca, P. University of Minho, Guimarães, Portugal, pp. 489-498
29. Vieira J. L. M. (1997). A discrete element model for the study of masonry structures. M.Sc. Thesis, Instituto Superior Técnico, Lisbon (in Portuguese)
30. Heyman, J. M. A. (1982). The masonry arch. Ellis Horwood
31. Lemos, J. V. (2006). Modelling of Historical Masonry with Discrete Elements. In Computational Mechanics – Solids, Structures and Coupled Problems, Eds. Mota Soares, C. A. Et al. Springer, pp. 375-391
32. Muralha (2000). Rock mechanics tests of the church of Serra do Pilar Monastery. Technical report. LNEC, Lisbon (in Portuguese)
33. Cavicchi, A. and Gambarotta, L. (2005). Collapse analysis of masonry bridges taking into account arch-fill interaction. Engineering Structures 27, pp. 605-615.
34. Gago, S. G., Alfaiate, J. and Almeida J. R. (2003). Numerical simulation of an experimental test of a masonry bridge. 7th Congresso de Mecânica Aplicada e Computacional. University of Évora, Portugal (in Portuguese)
35. Heyman, J.M.A. (1995). Teoría, historia y restauración de Estructuras de Fábrica. Instituto Juan de Herrera, Madrid